Tuning ON/OFF Ratios in Diarylethene-Based Single- and Bilayer Molecular Junctions

Imen Hnid, Mingyang Liu, Denis Frath, Sebastien Bellynck, Frederic Lafolet, Xiaonan Sun, Jean-Christophe Lacroix

Tuning ON/OFF ratios in diarylethene-based single- and bilayer molecular junctions

Authors: Imen Hnid, Mingyang Liu, Denis Frath, Sebastien Bellynck, Frederic Lafolet, Xiaonan Sun, Jean-Christophe Lacroix*

Université de Paris, ITODYS, CNRS, UMR 7086, 15 rue J-A de Baïf, 75205 Paris Cedex 13, France.

*Correspondence to: lacroix@univ-paris-diderot.fr

Abstract: Through electrochemical deposition, photoswitchable single and bilayer molecular junctions based on diarylethene (DAE) and bisthienylbenzene (BTB) layers were fabricated. The electrical characterization of closed and open forms of DAE were investigated by C-AFM for two different layer thicknesses fixed at 2-3 nm and 8-9 nm, i.e. below and above the direct tunneling limit. Both layers switch between high and low conductance modes ("ON" and "OFF" states) when irradiated by UV and visible light. ON/OFF ratios of 2-3 and 200-400 were obtained for 3 nm- and 9 nm-thick DAE MJs, respectively. Next, we prepared 9 nm-thick MJs using a bi-layer system. The first layer (5 nm) is based on BTB oligomers. The second layer (4 nm) is based on DAE oligomers. The impact of this first layer on the switchable properties of the system, and on the photoresponse of the 9 nm-thick DAE-based MJs has been studied. The DAE/BTB bilayer generates new electronic functions combining photoswitching and photorectification. The open form of DAE/BTB shows low conductance and asymmetric *I(V)* curves while the closed form shows symmetric *I(V)* curves and high conductance. More importantly, unprecedented ON/OFF current ratios of over 10 000 at 1 volt were reproducibly measured.

Photochromic molecules, i.e. molecules with two different forms (open/non-conjugated and closed/conjugated), which can be interconverted by light irradiation, have been proposed as building blocks for photoresistive switches in molecular electronics[1,2]. Many experiments have led to fundamental understanding of the transport characteristics in such systems, most of them have been limited to monolayers-based or single-molecule-based molecular junctions (MJs) where the dominant transport mechanism is direct tunneling[3–6]. In this regime, the photoswitching shows poor reversibility[7,8] and small ON/OFF ratios (less than two orders of magnitude) due to a strong molecule-electrode coupling which induces a quenching effects, [9–

[11] and it is only recently that a high ON/OFF ratio (around 100) with good reversibility was reported, using a strategy that decouples the active unit from the electrode [12]. When the thickness of the layer incorporated in a MJ is above 5 nm the main transport mechanism is hopping, which has a stronger molecular signature than tunneling [13–17]. A recent study, has compared the performances of photoactive devices in both regimes [18]. The studied MJs showed ON/OFF ratios of 10 and were not significantly affected by the length of the wire.

In this work, we first prepare photo switchable MJs using molecular layers based on photochromic diarylethene oligomers, grafted by diazonium salt electroreduction, and compare ON/OFF ratios for two different layer thicknesses corresponding to two different transport regimes, i.e. direct tunneling and hopping. Next, we prepared, using a bi-layer system, 9 nm-thick MJs, i.e. in the hopping transport regime. The first layer (5 nm) is based on bisthienylbenzene oligomers (BTB). The second layer (4 nm) is based on diarylethene oligomers (DAE). The impact of this first layer on the switchable properties of the system on the electronic behavior and on the photoresponse of the 9 nm-thick DAE-based MJs has been studied. Some of these results have already been separately published in ACS journal.[19,20]

1-(2-Bisthienyl)-4-aminobenzene (BTAB) and perfluoro-1,2-bis(2-(4-aminophenyl)-5-methylthien-4-yl)-cyclopentene (DAE-($C_6H_4NH_2)_2$) were synthesized by known procedures [8,21,22]. They both incorporate aniline groups for electrografting, but the first has thiophene units and the second has a dithienylethene (DTE) unit as the photochromic center (Figure 1a).

The electrochemical properties of DAE-$(C_6H_4NH_2)_2$ in solution was investigated by cyclic voltammetry (Figure 1b). Briefly, the open form shows one irreversible peak for aniline oxidation at 0.81 V/SCE (blue). The closed form shows two peaks, one reversible at 0.47 V/SCE and a second, weaker, irreversible peak at 0.87 V/SCE (red). The first peak is associated with the oxidation of the closed DAE core and the second is related to the oxidation of the amine unit. These results indicate that the HOMO of the closed form of DAE is (i) close to -5.6 eV while that of the open form is much lower; (ii) almost in resonance with that of BTB while that of the open form is way below.

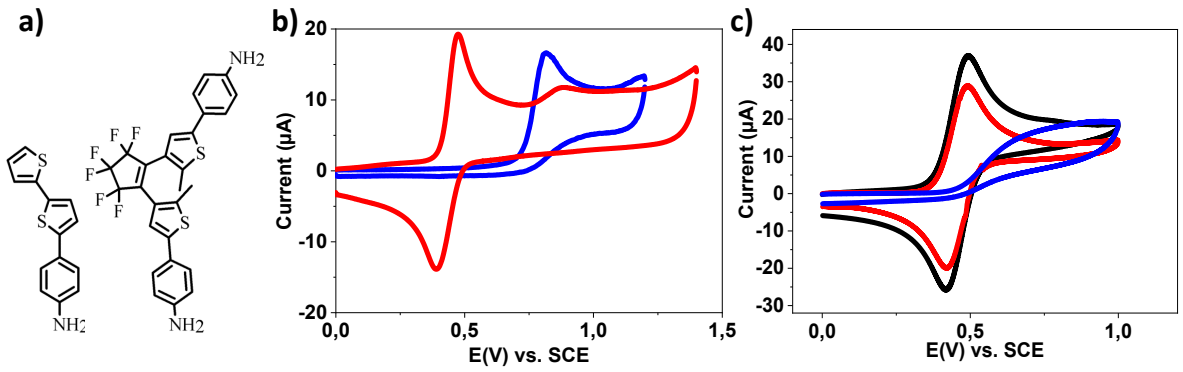

Figure 1. (a) 1-(2-Bisthienyl)-4-aminobenzene (BTAB) and perfluoro-1,2-bis(2-(4-aminophenyl)-5-methylthien-4-yl)-cyclopentene (DAE-$(C_6H_4NH_2)_2$. (b) CVs of DAE-$(C_6H_4NH_2)_2$ (red) open and (blue) closed form in oxidation range. (c) Ferrocene electrochemical responses (5 mM solution in ACN) (black) on bare and diarylethene-modified electrodes (red) before and (blue) after UV irradiation. Supporting electrolyte: 0.1 M $TBAPF_6^-$; scan rate 0.1 $V.s^{-1}$. Adapted with permission from reference [19]. Copyright (2020) American Chemical Society.

Then we grafted DAE-$(C_6H_4NH_2)_2$ onto GC or gold electrodes, generating the diazonium salt in situ by adding 10 equivalents of tBuONO. Details on the electrochemical conditions are given in Figure S1a, which shows the CV of the reduction of the diazonium salt of DAE in the open form. It displays an irreversible cathodic wave centered at -0.13 V/SCE, attributed to the reduction of the diazonium cation. During subsequent cycles, it progressively decreases. This behavior is common for the electroreduction of diazonium salts and indicates that an insulating organic layer has been deposited on the substrate. A similar procedure was used to create DAE/BTB layers. A 3-5 nm thick BTB layer was first grafted onto GC or gold as already described (Figure S1b, gray curve). Next, DAE was grafted onto the BTB/Au electrode using a similar procedure (Figure S1b, blue curve).

The electroactivity of the DAE-modified electrode was studied in the presence of a ferrocene redox probe before and after UV irradiation. Compared to the bare electrode (Figure 1c, black), the CV of ferrocene on the DAE-open modified electrode (Figure 1c, blue) does not show a reversible signal at the potential where ferrocene is usually oxidized. The layer formed on the electrode prevents the oxidation of the probe and the ferrocene signal is partially blocked, with an irreversible signal characterized by a ΔEp above 600 mV. After UV irradiation, ferrocene shows a reversible signal (Figure 1c, red) very close to that for a bare electrode (reversible signal with ΔEp close to 60 mV). Furthermore, this signal is at 0.47 V/SCE which is close to the redox signal of the closed form of DAE in solution. This indicates that some closed DAE units have been generated on the surface by irradiation. Such

units can act as electron relays or may generate pinholes in the initial layer, allowing ferrocene to be reversibly oxidized. The number of DAE units undergoing this switch is unknown but is high enough for the layer to become partially transparent and conductive towards ferrocene.

The bilayer system were also characterized by cyclic voltammetry (Figures S2 and S3). An exciting and unique result, demonstrated by electrochemistry, is that DAE/BTB/Au electrodes show double switching, one associated with the oligothiophene-based backbone, triggered by the applied potential and changing the conductivity of the layer (p-doping) and a second one, triggered by light, based on the interconversion of the photochromic DAE units, alternating between open/non-conjugated and closed/conjugated forms.

To characterize the layers by X-ray photoelectron spectroscopy (XPS), gold electrodes were modified by DAE and DAE/BTB layers. Figure S4 shows the XPS for the DAE and Figure 2 shows the XPS for the bilayer DAE/BTB. The survey XPS spectra show that peaks corresponding to fluorine, carbon, gold and sulfur are seen (Figure 2a and Figure S4a). The gold peaks are still observable, suggesting that the layer is less than 10 nm-thick.

The high-resolution spectrum of S2p displays the typical double peaks S2p½ and S2p3/2 attributed to the sulfur of the thiophene rings (Figure 2b and Figure S4b). The high-resolution spectrum of F1s shows a peak at 688 eV, which corresponds to fluorine atoms of the DAE (Figure 3c and Figure S4c). The high-resolution spectrum of C1s shows two main peaks at 285 eV and 291 eV attributed to aromatic carbon atoms and fluorine-bonded carbon atoms, respectively (Figure 3d and Figure S4d).

The atomic ratios obtained from the experimental XPS data and the theory for DAE single layer and BTB/DAE layers are presented in Figure 2e. For DAE layers, the calculated fluorine/sulfur ratio (F/S) is about 3.2 and the expected value is 3. The experimental (C/S) and (C/F) ratios are about 15 and 4.6, also in good agreement with the theoretical values of 13.5 and 4.5, respectively. For the DAE/BTB layers (F/S) (C/S) and (C/F) experimental ratios are 2.5, 14, and 5.5 respectively which indicates that (i) DAE is grafted on top of the BTB layer (BTB XPS signal does not contain Fluorine signal) (ii) the underlying BTB layer is still seen under XPS analysis. Figure 2e also depict the theoretical values of a layer with various BTB and DAE ratios (1BTB1DAE to 1BTB3DAE) and the atomic ratio for the latter are close to the experimental results. Overall, these results further that layers of DAE and DAE/BTB layers are easily formed on gold by diazonium electroreduction.

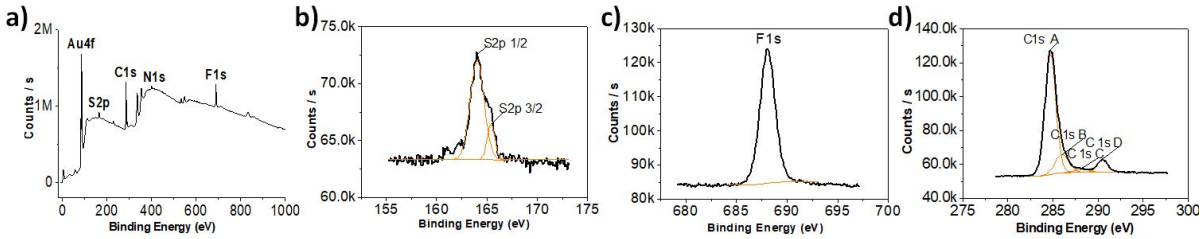

e)

Atomic ratio	DAE Layer experimental	DAE layer Theoretical values	DAE/BTB layer Experimental	Expected value 1BTB 1DAE	Expected value 1BTB 2DAE	Expected value 1BTB 3DAE
F/S	3,2	3	2,52	1,5	2	2,25
C/S	15	13,5	13,9	10,9	11,3	11,9
C/F	4,6	4,4	5,52	6,8	5,6	5,2

Figure 2. Characterization of DAE/BTB-modified gold surface (layer thickness 9 nm): (a) survey XPS. (b) High-resolution S2p XPS spectrum. (c) High-resolution F1s XPS spectrum. (d) High-resolution C1s XPS spectrum. (e) Atomic ratio calculated from experimental data and theory for DAE and BTB/DAE modified electrodes.

We then grafted these molecules onto gold microelectrode stripes (20 µm x 2 cm and 45 nm-thick on SiO_2/Si substrate). Different layer thicknesses were generated and measured by AFM using the cross-sections of the modified and bare gold stripes (figures 3).

Figure 3a shows an example of AFM statistical analysis in which we measured a thickness of 46 nm, and 49.1 nm for the bare gold (zero thickness is the Si/SiO_2 electrode) and the DAE-modified electrodes, respectively. An average thickness of 3.1 ±1 nm is found. Other DAE-modified electrode with an average thickness of 8.5 ±1 nm was also fabricated. Figure 3b shows another example were a first layer of BTB is grafted on gold (measured thickness of 44.4 nm and 49.3 on the bare and the BTB-modified electrode indicating an average thickness for the BTB layer of 5 nm) followed by the grafting of DAE on the BTB_{5nm}/Au/ electrode (measured thickness of 53.4 for the DAE/BTB/Au system deposited on the SiO_2/Si substrate indicating an average thickness for the DAE layer of 4 nm). The total thickness is thus 9±1 nm for the DAE/BTB layers.

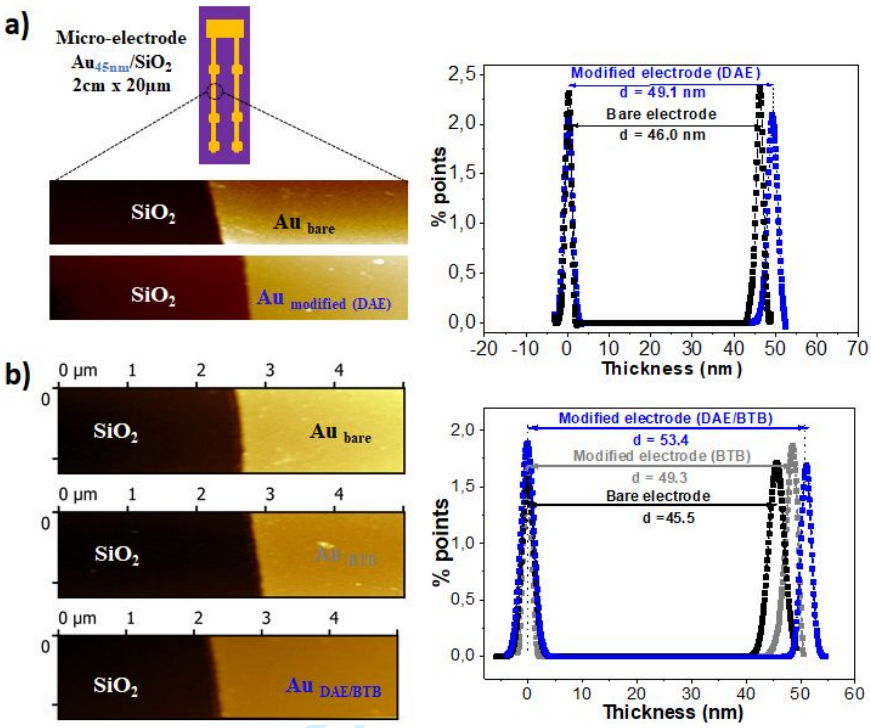

Figure 3. (a) AFM topography images of bare Au stripe and Au stripe functionalized by DAE molecules electrochemically deposited. Statistical analysis of the corresponding AFM images showing a film thickness of 3.1nm. (b) AFM topography images of bare Au stripe, Au stripe functionalized by DAE molecules and by DAE/BTB bilayer. Statistical analysis of the corresponding AFM images showing a film thickness of 9nm.

Next we investigated the electronic properties of DAE single layer for various thickness (3 ±1 nm and 8.5 nm ±1 nm) and DAE/BTB bilayer with total thickness of 9 ±1 nm. A C-AFM tip was used as a top electrode to create a molecular junction as depicted in Figure 4. The total thickness of 3 nm and 9 nm for DAE single layer has been chosen to compare the results in two different dominant transport regimes. i.e. direct tunneling and hopping for the 3 nm and 9 nm thick devices respectively while the 9 nm thick devices for DAE single layer and DAE ~4nm/BTB ~5nm bilayer have been chosen to study the effect of the underlying BTB layer on transport and photoswitching properties.

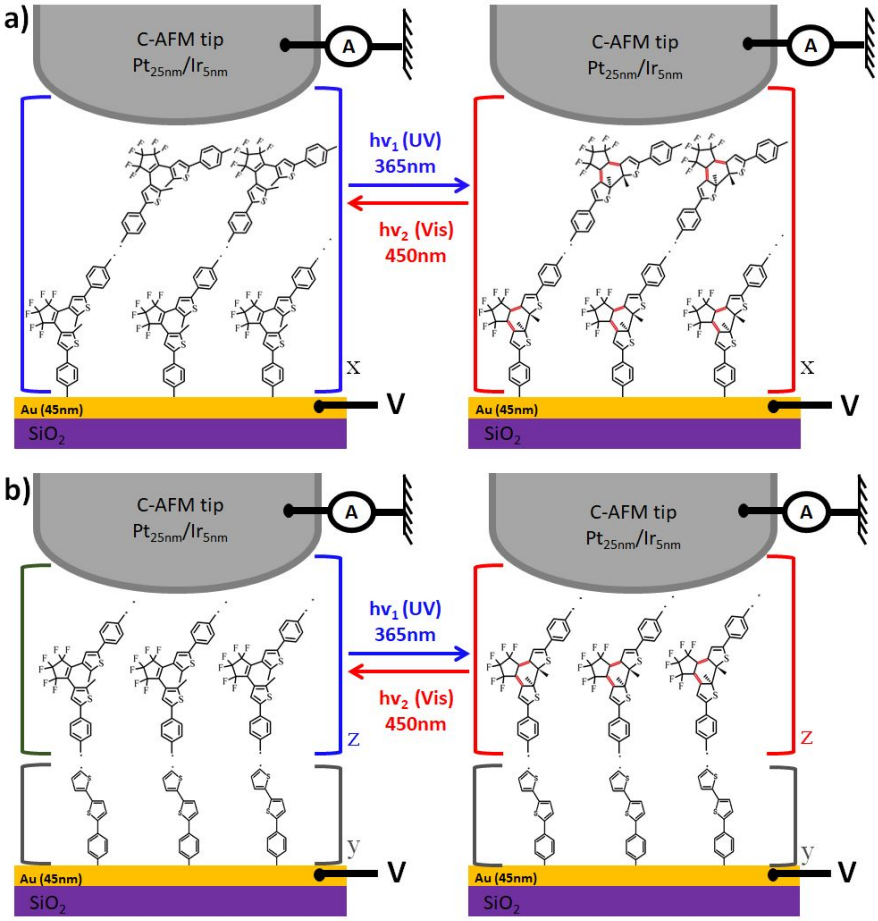

Figure 4. Schematic illustration of (a) $SiO_2/Ti_{2nm}/Au_{45nm}/oligo(DAE)_{8\text{-}9nm}$/CAFM tip ($Pt_{25nm}/Ir_{5nm}$) (b) $SiO_2/Ti_{2nm}/Au_{45nm}/oligo(BTB)_{4\text{-}5nm}/oligo(DAE)_{4nm}$/CAFM tip ($Pt_{25nm}/Ir_{5nm}$) molecular junction. x,y,z are numbers of repeating units of the oligomers which determine the thickness of the layer. The switch of the DAE units is turned ON by UV and OFF by visible light.

The current versus voltage *I(V)* data from these experiments are summarized in Figure 5. Each curve represents an average of 200 *I(V)* traces in several positions using the same applied force (~2.5 nN).

First, the measurements were performed on the initial state where the DAE units have been grafted in their stable open form. This form is associated with the OFF state (blue curve, Figure 5). Then, the junctions were irradiated by UV light (at 365 nm) for 1 hour in order to reach a photo stationary state with a high closed-form content. This form will be labelled the ON state in the following, as the conjugation extends over most of the photochrome (red curves, Figure 5). All MJs shows reversible behavior upon UV and Vis irradiation cycles.

A modest switch of the transport properties of the 3nm thick DAE single layer MJs is observed (Figure 5a) upon light irradiation and can be attributed to a change of the

isomerization state of the DAE layer. The junction is more resistive when the DAE units are in their open photostationary state. The current reaches 3 nA at 3 V (blue) while it reaches 9 nA at 3 V (red) in the ON state after irradiation with UV light (closed form). ON/OFF ratios are thus around 2-3 for this device. Such result is close to those reported by others when direct tunneling is the dominant transport regime.[3,9,11,18,23] Such low ON/OFF ratio can be attributed to partial quenching of the isomerization by the electrodes, to incomplete photoisomerization, which always occurs in multiphotochromic systems[24], and to the fact that in the direct tunneling regime a small molecular signature on transport is observed in the strong coupling regime.

Figure 5b shows the average *IV* curves of the 9nm thick DAE single layer MJ before (blue) and after (red) UV irradiation. These curves show that the current now strongly depends on the isomerization state of the layer. The current is only few pA at 3 V when the layer consists of DAE oligomers mainly in their open form, while it reaches 1 to 2 nA at 3 V when the layer has been UV-irradiated. An important result is that ON/OFF ratios between 200 and 400 are now obtained thanks to the highly resistive behavior of the 9 nm thick DAE MJ in its OFF state. Dominant transport mechanism in this 9 nm thick layer cannot be direct tunneling and transport is likely done by hopping Such results confirm that in the hopping regime a stronger molecular signature on transport can be observed.[13,14,25–28]

Figure 5c shows the average *I(V)* curves of the 9nm thick DAE/BTB bilayer MJ before (blue) and after (red) UV irradiation The current does not exceed a few picoamps at 1 V (note that it is close to the limit of detection of the measurement system) while it reaches 9 nA at 1 V in the ON state after irradiation with UV light (closed form). Switching to the ON state shows a saturated *I(V)* curve above 1.2 V, indicating that the junction conductance is so high that the C-AFM amplifier can no longer measure the current. In other words, the ON state is much more conductive than in 9 nm thick DAE layer while the OFF state is as resistive. As a consequence, ON/OFF ratio reaches an unprecedented value of 10 000 at 1 V. Figure 5d expands the voltage range to +3 V and shows that the *I(V)* curve in the OFF state is not symmetrical anymore (upper inset) and that this device rectifies the current, the preferred current direction being obtained for negative voltage applied to the bottom electrode.

Finally, Figure SI5 shows the *I(V)* curves recorded between -3 and +3 V using and C-AFM equipped with a system allowing *I(V)* measurements with current varying over seven orders of magnitude. In the ON state the current reaches 90 nA at -3 and +3V and the *I(V)* curve is symmetrical with no preferred direction, whereas in the OFF state it is only few picoamps at

+3 V, and -1.8 nA at -3 V. Rectification in the OFF state is best seen in the upper inset of Figure 5c; the rectification ratio reaches 200 at +3 V. The ON/OFF ratio of the MJ remains at 10 000 at 3 V while it decreases to 50 at -3 V.

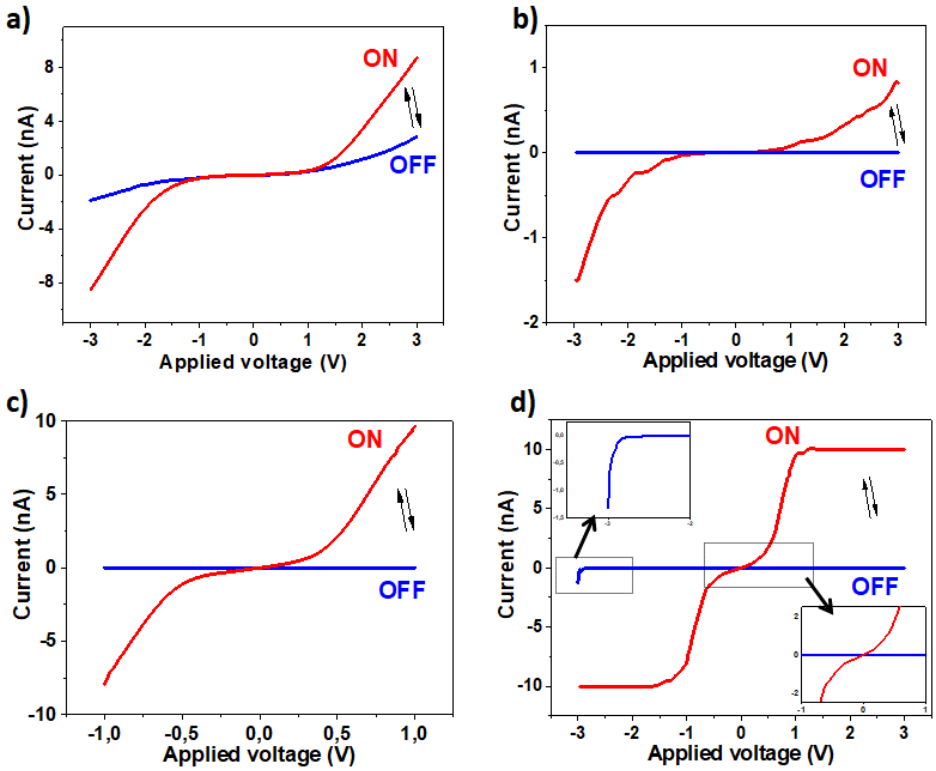

Figure 5. Transport characteristics of the (a) 3 nm and (b) 9 nm thick DAE single layer MJs and (c) 9 nm thick DAE/BTB bilayer MJs measured by C-AFM before (blue and blue curves) and after (red curves) UV irradiation at room temperature. Upper inset, zoom on the OFF state *I(V)* curve, lower inset, zoom around zero volt OFF and ON state *I(V)* curves. Adapted with permission from references [19 and 20]. Copyright (2020 and 2021) American Chemical Society.

These results demonstrate that the transport properties of the devices are considerably tuned by the first BTB layer, acting as an electroswitchable molecular spacer (see Figure S2 and S3), between the DAE units and the bottom electrode, while keeping the same overall junction thickness (~9 nm). New electronic functions combining photorectification and photoswitching are observed. *I(V)* curves of the bilayer in the off state are asymmetric with high rectification at 3V. Upon irradiation and switching of the DAE layer to the ON state rectification disappear. More importantly, giant ON/OFF ratios above 10 000 between -1 and +1V and at +3V are obtained. The ON state of the bilayer devices is much more conductive than that of the DAE_{9nm} single-layer devices while the conductances of the OFF states are similar. BTB electroswitchable properties (p-doping) which can reduce the effective transport distance and resonance between the HOMO levels of BTB and DAEc explains the high

conductance of the ON state of the DAEc/BTB MJs. The ON/OFF ratio may also be enhanced by the BTB spacer which probably limits the quenching effects[7,8,29] of the bottom electrode on the yield of the DAE photoswitch interconversion.

Overall: this work shows that molecules with electro- and photoswitchable properties can be combined in solid-state devices to develop new and key components for future nanoelectronics. These easily reproducible results present the highest ON/OFF conductance ratio obtained in solid-state photoswitches based on photochromic molecules Electrochemical engineering designed to control coupling between molecules has been the key in constructing photorectifiers and photoelectrical switches.

Acknowledgments:

This work was supported by the Agence Nationale de la Recherche ANR (France) is gratefully acknowledged for its financial support of this work (ANR-19-CE09 APMJ). We thank Dr. John S. Lomas for editing our manuscript.

Data and materials availability:

All data is available in the main text or the supplementary materials.

Supplementary Materials:

Materials and Methods

Figures S1-S6

References and Notes:

1. M. Irie, T. Fukaminato, K. Matsuda, and S. Kobatake, *Chem. Rev.*, **114**, 12174–12277 (2014) https://doi.org/10.1021/cr500249p.

2. X. Huang and T. Li, *J. Mater. Chem. C*, **8**, 821–848 (2020).

3. J. He et al., *Nanotechnology*, **16**, 695–702 (2005).

4. K. Smaali et al., *ACS Nano*, **4**, 2411–2421 (2010).

5. S. Karpe et al., *Chem. Commun.*, **46**, 3657–3659 (2010).

6. C. Jia et al., *Angew. Chemie - Int. Ed.*, **52**, 8666–8670 (2013).

7. D. Dulić et al., *Phys. Rev. Lett.*, **91**, 1–4 (2003).

8. A. C. Whalley, M. L. Steigerwald, X. Guo, and C. Nuckolls, *J. Am. Chem. Soc.*, **129**, 12590–12591 (2007).

9. N. Katsonis et al., *Adv. Mater.*, **18**, 1397–1400 (2006).

10. J. M. Mativetsky et al., *J. Am. Chem. Soc.*, **130**, 9192–9193 (2008).

11. K. Uchida, Y. Yamanoi, T. Yonezawa, and H. Nishihara, *J. Am. Chem. Soc.*, **133**, 9239–9241 (2011).

12. C. Jia et al., *Science (80-.).*, **352**, 1443–1445 (2016).

13. Q. van Nguyen et al., *J. Am. Chem. Soc.*, **139**, 11913–11922 (2017).

14. S. Y. Sayed, J. A. Fereiro, H. Yan, R. L. McCreery, and A. J. Bergren, *Proc. Natl. Acad. Sci. U. S. A.*, **109**, 11498–503 (2012).

15. I. Hnid et al., *J. Phys. Chem. C*, **124**, 26304–26309 (2020).

16. Y. Han and C. A. Nijhuis, *Chem. – An Asian J.*, **15**, 3752–3770 (2020).

17. Y. Han et al., *Adv. Sci.*, **8**, 2100055 (2021).

18. D. Taherinia and C. D. Frisbie, *J. Phys. Chem. C*, **120**, 6442–6449 (2016).

19. I. Hnid, D. Frath, F. Lafolet, X. Sun, and J.-C. Lacroix, *J. Am. Chem. Soc.*, **142**, 7732–7736 (2020).

20. I. Hnid et al., *Nano Lett.*, **21**, 7555–7560 (2021)

21. C. Fave et al., *J. Am. Chem. Soc.*, **129**, 1890–1891 (2007).

22. G. Trippé-Allard and J. C. Lacroix, *Tetrahedron*, **69**, 861–866 (2013).

23. J. M. Mativetsky et al., *J. Am. Chem. Soc.*, **130**, 9192+ (2008).

24. A. Perrier, F. Maurel, and D. Jacquemin, *Acc. Chem. Res.*, **45**, 1173–1182 (2012).

25. H. Yan et al., *Proc. Natl. Acad. Sci. U. S. A.*, **110**, 5326–5330 (2013).

26. Q. Van Nguyen et al., *J. Am. Chem. Soc.*, **140**, 10131–10134 (2018).

27. A. Bayat, J. C. Lacroix, and R. L. McCreery, *J. Am. Chem. Soc.*, **138**, 12287–12296 (2016).

28. U. M. Tefashe, Q. Van Nguyen, F. Lafolet, J.-C. Lacroix, and R. L. McCreery, *J. Am. Chem. Soc.*, **139**, 7436–7439 (2017).

29. A. Staykov, D. Nozaki, and K. Yoshizawa, *J. Phys. Chem. C*, **111**, 3517–3521 (2007).

TOC